# Study on the Preparation and Properties of Fe-tailings Based Foamed Glass-ceramics

**Pengwei Li**
Northeastern University
**S.H. Luo** ( tianyanglsh@163.com )
School of Materials Science and Engineering, Northeastern University, Shenyang 110819, PR China
https://orcid.org/0000-0002-4517-3728
**Qing Wang**
Northeastern University
**Pudong Zhang**
Northeastern University
**Yahui Zhang**
Northeastern University
**Xin Liu**
Northeastern University
**Jinsheng Liang**
Hebei University of Technology
**Xinhui Duan**
Hebei University of Technology

**Research Article**

**Keywords:** Iron tailings, Foamed glass-ceramic, Base glass, CaCO3, Foaming

**DOI:** https://doi.org/10.21203/rs.3.rs-142227/v1

# Abstract

Traditional building materials have disadvantages such as high pollution and high energy consumption, so it is particularly important to develop new environmentally friendly materials. In this paper, foamed glass-ceramics are prepared by high-temperature melting method with iron tailings, blast furnace slag, and desulfurization slag as the main raw materials, and $CaCO_3$ as foaming agent. The effects of three kinds of basic glass scheme, the content of the foaming agent and heat treatment system on the degree of crystallization, micro-morphology, and crystal phase composition of foamed glass-ceramics are studied. The nucleation temperature and crystallization temperature of the basic glass are determined by differential thermal analysis curve to be 730 ℃ and 1000 ℃, respectively. Orthogonal experiments show that the optimal composition ratio of the prepared base glass is CaO: 22.25 wt.%, MgO: 4.57 wt.%, $Al_2O_3$: 6.19 wt.%, $SiO_2$: 41.8 wt.%. The optimized scheme is based on a base glass prepared with 45 wt.% iron tailings, 25 wt.% blast furnace slag, and 30 wt.% desulfurization slag, added with 10% $CaCO_3$ and sintered to 1000 °C for 3 h. The bending strength, fracture toughness, and elastic modulus are 95.73 Mpa, 53.09 $Mpa{\cdot}m^{1/2}$, 28023.55 Mpa, respectively.


# 1. Introduction

Iron tailings are solid waste residues that are discharged to tailings pond after cleaning and screening after iron-bearing ore beneficiation [1]. At present, more than 90% of iron tailings in China are stacked outdoors, occupying a large amount of arable land, which has caused serious environmental pollution, and only less than 10% of iron tailings are comprehensively utilized in construction materials [2, 3]. Therefore, the development of products with higher added value has far-reaching significance for the comprehensive secondary utilization of iron tailings. Because iron tailings are rich in chemical components such as $SiO_2$, CaO, MgO, and $Al_2O_3$, which can be used to prepare glass-ceramics with various properties, which can not only reduce environmental pressure and realize the reuse of waste resources but also reduce the development of productions of new raw material cost.

Glass-ceramics is a kind of ceramic material in which crystals and glass phases are uniformly distributed by controlling the crystallization behavior of the basic glass [4]. The difference between glass-ceramic and ordinary glass is that it has a regular crystal structure, and the difference from ceramic materials is that its crystal structure is more refined [5]. Foam glass is prepared from glass powder, foaming agent, modified additive, and foam stabilizer. Foam glass has the characteristics of fire-resistance [6], waterproof [7], non-toxic [8], anti-corrosion [9], anti-mite [10], non-aging [11], non-radioactive[12], insulation [13], anti-magnetic wave [14], and high mechanical strength [15, 16]. Foamed glass-ceramics is a new type of porous material, which is prepared of basic glass, non-metallic minerals as the main raw materials by adding foaming agents, nucleating agents, and some necessary chemical reagents through preheating, sintering, foaming, crystallization, annealing [17, 18].

Comprehensive utilization of iron tailings can not only solve the problems of massive tailings accumulation and environmental pollution but also recycle resources. In this paper, foamed glass-ceramics

are prepared from industrial wastes such as iron tailings, blast furnace slag, and desulfurization slag. No other chemical reagents are introduced during the experiment, which not only greatly reduced the production cost, but also improved the mechanical properties of the products. This work has good economic and environmental benefits.

## 2. Experimental

# 2.1 Experimental Materials

All the three raw materials used in the experiment were industrial waste residue, and the iron tailings were from Miaogou iron mine in Qinhuangdao, which was hard and brittle and gray-black. Blast furnace slag was a gray-black block and spherical, porous, and brittle. Desulfuration slag was khaki powder. The raw materials were analyzed by X-ray fluorescence spectrometer, and the results were shown in Table 1. The foaming agent used in the experiment was analytical reagent grade $CaCO_3$.

**Table 1**

The main chemical composition of iron tailings, blast furnace slag, and desulfuration slag (wt.%)

| Raw materials | $SiO_2$ | $Fe_2O_3$ | $Al_2O_3$ | MgO | CaO | $Na_2O$ | $K_2O$ | $SO_3$ | $TiO_2$ | Other |
|---|---|---|---|---|---|---|---|---|---|---|
| Iron tailings | 75.47 | 8.34 | 5.99 | 4.094 | 2.86 | 1.36 | 1.056 | 0.212 | 0.151 | 0.458 |
| Blast furnace slag | 28.2 | 1.328 | 12.88 | 10.26 | 35.8 | 0.55 | 0.54 | 1.73 | 8.233 | 0.419 |
| Desulfuration slag | 2.72 | 1.198 | 0.913 | 0.551 | 39.9 | 1.51 | 0.551 | 47.94 | 2.536 | 2.131 |

# 2.2 Scheme design of basic glass

The composition of base glass and heat treatment system were the main factors affecting the crystallization ability, crystal type, and mechanical properties of glass-ceramics. Figure 1 showed the phase diagram of the $CaO$-$Al_2O_3$-$SiO_2$ ternary system containing 10 wt.% MgO [19]. The basic glass composition was designed according to the composition in the pyroxene region and near the eutectic point, because the melting point in the system at the eutectic point was low, which was beneficial to the melting of the basic glass and can achieve the purpose of reducing energy consumption. In this experiment, three groups of basic glass schemes were designed, which fully compensate for the shortage of related components of iron tailings. The raw material ratios of the three groups of basic glass were shown in Table 2.

**Table 2**

Scheme of base glass (wt.%)

| Composition | $SiO_2$ | $Al_2O_3$ | CaO | MgO | $Na_2O/K_2O$ | $Fe_2O_3$ | $TiO_2$ |
|---|---|---|---|---|---|---|---|
| Scheme A | 45.47 | 6.45 | 20.60 | 4.90 | 2.00 | 10.80 | 2.30 |
| Scheme B | 41.80 | 6.19 | 22.25 | 4.57 | 2.65 | 4.45 | 2.13 |
| Scheme C | 49.45 | 6.45 | 18.56 | 5.08 | 1.88 | 5.12 | 2.13 |

# 2.3 Experimental method

Preparation of foamed glass-ceramics: Firstly, iron tailings, blast furnace slag, and desulfuration slag were ground into powder by vibration milling. Then, it was sieved by a 200-mesh square-hole sieve and dried in a vacuum drying oven at 110 ℃ for 12 h. According to the composition of basic glass, the powder with the corresponding mass was weighed and mixed evenly. Put 90 g basic glass powder into corundum crucible, then put it into high-temperature resistance furnace, raise the temperature from room temperature to 1450 ℃ at the rate of 7 ℃·$min^{-1}$, and keep it for 60 min. After the basic powder was sintered, water quenching treatment was carried out. The water-quenched basic glass was dried in an oven at 110 ℃ for 12 h. The dried glass powder was put into an electromagnetic sample preparation ore crusher, ground, and sieved. Weigh 30 g of basic glass powder and foaming agent, and put them into a ball milling tank for grinding and mixing evenly. Put the powder into a tableting mold and press it into a rectangular parallelepiped of 4.49 × 5 × 5.1 mm by a tablet press. Put the ceramic tray filled with samples into a high-temperature resistance furnace, raise the temperature to nucleation and foaming temperature according to a suitable heating system, and keep the temperature for a certain time. After the sample was cooled to room temperature with the furnace, the sample was cut into a specific shape with a wire cutting machine to obtain foamed glass-ceramics.

# 2.4 Material characterization

Differential thermal analysis (DTA) of the samples was measured by a thermogravimetric analyzer (Setsy Evolution) under an argon atmosphere. The test temperature ranged from 50 to 1400 °C, and the heating rate was 10 °C·$min^{-1}$. X-ray diffraction (XRD) characterization was carried out with a diffractometer DX-2500 (Dandong, China), using CuKα radiation (λ = 0.154056 nm, voltage 40 kV, and current 30 mA), with a scanning speed of 4.8°·$min^{-1}$ and a recorded range from 10 to 90°. The morphology of all samples was observed by scanning electron microscopy (SEM, Phenom XL). X-ray fluorescence spectroscopy (XRF, XRF-1800, Shimadzu Co., Ltd., Japan) was used to detect the main chemical components of raw materials. The specific surface area and pore size distribution were measured by the Brunauer-Emmett-Teller (BET) multipoint method using a specific surface area analyzer (SSA-4000).

## 3. Results And Discussion

# 3.1 Basic glass

The XRD patterns of the three groups of basic glasses are shown in Fig. 2(a). It can be seen from the figure that the sintered basic glass powder is mainly amorphous. By comparison, it is found that the basic glass prepared by scheme 1 has a small amount of crystallization. The appearance of crystallization makes it easy for the basic glass to generate internal stress in the subsequent heat treatment process, which adversely affects the properties of foamed glass-ceramics. Therefore, considering the stability of the basic glass comprehensively, it is more appropriate to choose schemes 2 and 3. The DTA curve of the basic powder shown in Fig. 2(b) shows that the nucleation temperature of the basic glass powder is about 730 ℃, and the crystallization temperature is about 1000 ℃.

According to the trial sintering experiment and the differential thermal analysis, the following nine groups of orthogonal experiments (Table 3) are determined to study the factors such as the amount of foaming agent and the heat treatment system.

**Table 3**

Results of the orthogonal experiment

| Factor Group | Scheme | $CaCO_3$ content (wt.%) | Crystallization temperature (°C) | Holding time (h) | Bending strength (Mpa) |
|---|---|---|---|---|---|
| 1 | A | 10% | 1000 | 1 | 78.172 |
| 2 | A | 20% | 1050 | 2 | 35.555 |
| 3 | A | 30% | 1100 | 3 | 13.815 |
| 4 | B | 10% | 1050 | 3 | 81.460 |
| 5 | B | 20% | 1100 | 1 | 42.137 |
| 6 | B | 30% | 1000 | 2 | 15.233 |
| 7 | C | 10% | 1100 | 2 | 76.195 |
| 8 | C | 20% | 1000 | 3 | 43.630 |
| 9 | C | 30% | 1050 | 1 | 11.037 |
| k1 | 42.514 | 78.609 | 45.675 | 43.782 | / |
| k2 | 46.273 | 40.44 | 42.684 | 42.324 | / |
| k3 | 43.62 | 13.358 | 44.049 | 46.3 | / |
| R | 3.759 | 65.251 | 2.911 | 3.976 | / |
| Factor priority | $CaCO_3$ content > Holding time > Scheme > Crystallization temperature | | | | |

# 3.2 Foamed glass-ceramics

### 3.2.1 *The content of foaming agent*

The degree of dispersion of bubbles in foamed glass-ceramics depends to a certain extent on the uniformity of the dispersion of the foaming agent in the basic glass powder [20]. Furthermore, the amount of foaming agent incorporated will greatly affect the distribution of bubbles. When the amount of foaming agent is too high, the number of microbubbles increases, which leads to the convergence of a large number of rising bubbles, and makes the foaming distributed in layers. The crystallization temperature of the basic glass powder also restricts the type and amount of foaming agent. The transformation of glass powder from solid to molten is an endothermic process. The DTA curve shows that the nucleation temperature and crystallization temperature are about 730 ℃ and 1000 ℃. According to comprehensive analysis, $CaCO_3$ is selected as the foaming agent. This is because the foaming temperature of $CaCO_3$ is compatible with the nucleation temperature and crystallization temperature of the basic glass powder. According to the research on the trial sintering experiment, the content of $CaCO_3$ is selected as 10%, 20%, and 30 wt.%, respectively.

### 3.2.2 *Crystallization temperature*

The proper foaming temperature can control the size of the bubbles and the uniformity of the cell distribution. The foaming temperature of foamed glass-ceramics should be equivalent to the nucleation temperature of the melt, so the foaming temperature should be 730 ℃. The growth of crystal grains is mainly completed in the crystallization stage, and the crystallization temperature is too high or too low, which is not conducive to the precipitation of crystals. The crystallization temperature is preferably 1000 ℃, 1050 ℃, and 1100 ℃, respectively.

### 3.2.3 *Holding time*

The holding time mainly affects the pore size and the dispersion degree of the bubbles. Too long holding time will cause small bubbles to rise. The foaming agent has just begun to decompose into small bubbles, and then it has entered the cooling stage, which makes the foaming process end prematurely, resulting in large bulk density and poor mechanical properties of products [21]. The crystallization time will directly affect the size of the crystal grains, thereby affecting the properties of the foamed glass-ceramics. The research shows [22] that in order to obtain enough grain length, the holding time should not be less than 60 min. In summary, in this study, the foaming holding time is 60 min, and the crystallization holding time is 60 min, 120 min, and 180 min, respectively.

## 3.3 Orthogonal experiment analysis

Nine groups of orthogonal foamed glass-ceramics are used to test their bending strength, fracture toughness, and elastic modulus, to explore the effect of foaming agent content and heat treatment system on the mechanical properties of foamed glass-ceramics. The trends of the three mechanical properties are shown in Fig. 3 (a-c). According to the results shown in the trend picture, it can be seen that the bending strength, fracture toughness, and elastic modulus of foamed glass-ceramics show a decreasing trend with the increase of calcium carbonate content. This is because with the increase of foaming agent content, the

number of large pores and connected pores will increase, resulting in uneven foaming, and the mechanical properties of the samples will become worse. Moreover, the effects of crystallization temperature and holding time in the heat treatment system on bending strength and fracture toughness show a trend of decreasing at first and then increasing. In general, the bending strength of the glass-ceramic sample will increase with the increase of its crystallinity within a certain range. This is because according to the microcrack strength theory proposed by Griffith [23], the critical strength of crystals can be expressed as a large number of growth in the glass body, which leads to a large number of uneven surfaces on the fault section, resulting in higher fracture surface energy. It can be seen from the following formula that the increase of fracture surface energy will improve the strength of the material.

$$\sigma=(E\cdot\gamma/\pi C)^{1/2}$$

Where $E$ is the elastic modulus (GPa), γ is the fracture surface energy, ($J\cdot m^{-2}$); $C$ is the critical length of microcracks (mm).

According to the mechanical properties and the range analysis of nine groups of the orthogonal experiments, comprehensive considerations, the second group of basic glass is selected as the optimal scheme, that is, the calcium carbonate content is 10 wt.%, and the crystallization temperature is 1000 ℃. The holding time is 3 h.

# 3.4 Phase analysis

Figure 3d is the XRD pattern of the orthogonal experiment group. The results shown in the pattern show that the crystal type of the nine groups of samples is a single diopside phase ($CaMgSi_2O_6$). With the increase of the crystallization temperature and holding time, the intensity of the diffraction peaks of the samples increased continuously (1–3 experimental groups). There are some abnormal peaks in group 4, which may be mixed with a small amount of impurities. With the increase of crystallization temperature, the diffraction peak intensity of samples increases at first and then decreases, which is because the driving force for crystallization provided by the external temperature field decreases due to the short crystallization time [24], resulting in insufficient conditions for the crystal nucleus to grow up, which leads to the low crystal content of the crystallized samples. With the extension of the crystallization time, the driving force of crystallization also increases, the crystal nucleus fully develops and grows, and the crystal content of the sample after crystallization is higher. Therefore, the diffraction peak intensity of the sample will increase with the increase of the crystallization temperature within a certain range, but an excessively high crystallization temperature will cause the sample to remelt and suck back during the crystallization process, which leads to the increase of glass phase content, the diffraction intensity of the crystallization peak decreases.

# 3.5 Microscopic morphology analysis

The experimental results shown in Fig. 4 show that sample No.1 has a strong crystallization ability, and the formed crystals are massive, dense, and uniform, attached to the glass substrate, and the pore distribution is also relatively uniform. The crystallization ability of No.2, 3, and 5 samples is insufficient, a few massive

crystals are precipitated, and the number of nucleation is not much, and the pores are large. Sample No.4 precipitated some massive crystals, with dense pore distribution and honeycomb shape. Sample No.6 precipitates a lot of crystals, which are granular, massive, and a small number of flakes, and the pores are evenly distributed. Sample No.7 has large pores and sparse distribution, and the precipitated crystals are massive and evenly distributed. Sample No.8 is ideal, with many and dense precipitated crystals, most of which are massive, and the pore distribution is relatively dense. The morphology of the No.9 sample is dominated by massive crystals, some of which are inserted into the glass matrix in sheet form and wrapped by massive crystals, with large pores and uniform distribution. SEM analysis shows that with the increase of nucleation temperature and nucleation time, the nucleation process of the glass matrix is relatively sufficient, and the number of nuclei and the content of the crystal phase of the samples increase. With the extension of the crystallization time and the increase of the crystallization temperature, the content of the main crystal phase will also increase, and the crystal grains of the main crystal phase aluminum diopside are interlaced with each other, and the arrangement is more uniform and dense.

## 3.6 Optimization scheme

Combined with the mechanical properties obtained by orthogonal experiment, XRD pattern, and SEM morphology analysis results, it can be known that the optimal scheme for synthesizing foamed glass-ceramics is to select the second group of basic glass, with $CaCO_3$ content of 10 wt.%, the crystallization temperature of 1000 ℃ and holding time of 3 h. The XRD pattern of this group of samples shows that the main crystal phase is diopside ($CaMgSi_2O_6$), and the diffraction peak intensity is high, as shown in Fig. 5c. The SEM image of the sample shows that the precipitated massive crystal grains are more and evenly distributed, and the pore distribution is relatively dense (Fig. 5d). The adsorption-desorption isotherm curve of the sample shows type III, the multi-point BET specific surface area is 3.77 $m^2 \cdot g^{-1}$, the single-point total pore volume is 0.013491 cc/g, and the single-point average pore radius is 217.80 Å (Fig. 5a-b). The mechanical properties of the samples prepared by the optimal scheme show that the bending strength, fracture toughness, and elastic modulus are 95.73 Mpa, 53.09 $MPa \cdot m^{1/2}$, and 28023.55 Mpa, respectively, which are superior to other orthogonal experimental groups, and the experimental results are consistent with the theoretical analysis of XRD and SEM.

## 4. Conclusion

In this work, foamed glass-ceramics are prepared by high-temperature melting method with iron tailings, blast furnace slag, and desulfurization slag as main raw materials and calcium carbonate as the foaming agent. The main results are summarized as follows:

(1) The optimal raw material ratio for preparing basic glass is CaO: 22.25%, MgO: 4.57%, $Al_2O_3$: 6.19%, $SiO_2$: 41.8%.

(2) The XRD analysis shows that the samples prepared under different heat treatment regimes are all a single diopside phase ($CaMgSi_2O_6$).

(3) The SEM image analysis shows that extending the crystallization time and increasing the crystallization temperature can increase the content of the main crystalline phase, and diopside grains in the main crystalline phase are staggered and arranged more uniformly and densely.

(4) The optimal process for preparing foamed glass-ceramics is to select the second group of basic glass, with $CaCO_3$ content of 10 wt.%, the crystallization temperature of 1000 ℃, and the crystallization time of 3 h. At this time, the bending strength of the sample is 95.73 Mpa, the fracture toughness is 53.09 $Mpa{\cdot}m^{1/2}$, and the elastic modulus is 28023.55 Mpa.

## Declarations

# Acknowledgments

This work was financially supported by the National Natural Science Foundation of China (No.51874079, 51674068, 51804035), Natural Science Foundation of Hebei Province (No.E2018501091, E2020501001), Hebei Province Key Research and Development Plan Project (No.19211302D), The Fundamental Research Funds for the Central Universities (No. N172302001, N182312007, N182306001, N2023040), Research Project on the Distribution of Heavy Metals in Soil and Comprehensive Utilization Technology of Tailings in Typical Iron Tailing Reservoir Areas of Hebei Province (No.802060671901).

Special thanks are due to the instrumental or data analysis from Analytical and Testing Center, Northeastern University.

## References

1. Tang C, Li K, Ni W et al (2019) Recovering iron from iron ore tailings and preparing concrete composite admixtures. Minerals 9:232
2. Li PW, Luo SH, Wang YF et al (2021) Cleaner and effective recovery of metals and synthetic lithium-ion batteries from extracted vanadium residue through selective leaching. J Power Sources 482:228970
3. Wang Q, Gao CL, Zhang WX et al (2019) Biomorphic carbon derived from corn husk as a promising anode materials for potassium ion battery. Electrochim Acta 324:134902
4. Prasad A, Basu A (2013) Dielectric and impedance properties of sintered magnesium aluminum silicate glass-ceramic. J Adv Ceram 2:71–78
5. Deubener J, Allix M, Davis MJ et al (2018) Updated definition of glass-ceramics. J Non-cryst Solids 501:3–10
6. Takeda H (2003) A model to predict fire resistance of non-load bearing wood-stud walls. Fire Mater 27:19–39
7. Suvorova OV, Makarov DV (2019) Foam glass and foam materials based on ash-slag wastes from thermal power plants (Review). Glass Ceram 76:188–193

8. Hisham NA, Zaid MH, Saparuddin DI et al (2020) Crystal growth and mechanical properties of porous glass-ceramics derived from waste soda-lime-silica glass and clam shells. J Mater Res Technol 9:9295–9298
9. Li DW, Wang HY, Liu Y et al (2019) Large-scale fabrication of durable and robust super-hydrophobic spray coatings with excellent repairable and anti-corrosion performance. Chem Eng J 367:169–179
10. Makert GR, Vorbrüggen S, Krautwald JME et al (2016) A method to identify protein antigens of dermanyssus gallinae for the protection of birds from poultry mites. Parasitol Res 115:2705–2713
11. Altayan MM, Ayaso M, Darouich TA et al (2020) The effect of increasing soaking time on the properties of premixing starch–glycerol–water suspension before melt-blending process: comparative study on the behavior of wheat and corn starches. Polym Bull 77:1695–1706
12. Jin T, Mar D, Kim D et al (2020) Reactions during conversion of simplified low-activity waste glass feeds. Thermochim Acta 694:178783
13. Yatsenko EA, Smolii VA, Gol'tsman BM et al (2019) Optimal fractional composition of batch for synthesis of foam-glass materials based on diatomite from the chernoyarskoe deposit. Glass Ceram 75:391–393
14. Shi SM (2014) Laying the ground of indoor restrooms by using foam glass and waterproof coating. Adv Mater Res 989:260–263
15. Yan S, Pan Y, Wang L et al (2018) Synthesis of low-cost porous ceramic microspheres from waste gangue for dye adsorption. J Adv Ceram 7:30–40
16. Păunescu L, Drăgoescu MF, Axinte SM (2020) High mechanical strength porous material used as a foam glass gravel experimentally manufactured from glass waste by an unconventional technique. Constructii 21:54–62
17. Sasmal N, Garai M, Karmakar B (2015) Preparation and characterization of novel foamed porous glass-ceramics. Mater Charact 103:90–100
18. Krivoshapkina EF, Krivoshapkin PV, Vedyagin AA (2017) Synthesis of $Al_2O_3$–$SiO_2$–MgO ceramics with hierarchical porous structure. J Adv Ceram 6:11–19
19. Mao H, Hillert M, Selleby M et al (2006) Thermodynamic Assessment of the CaO–$Al_2O_3$–$SiO_2$ System. J Am Ceram Soc 89:298–308
20. Ewais EMM, Attia MAA, Amir AAM et al (2018) Optimal conditions and significant factors for fabrication of soda lime glass foam from industrial waste using nano AlN. J Alloy Compd 747:408–415
21. Liu T, Tang Y, Li Z et al (2016) Red mud and fly ash incorporation for lightweight foamed ceramics using lead-zinc mine tailings as foaming agent. Mater Lett 183:362–364
22. Shen Z, Johnsson M, Zhao Z et al (2002) Spark plasma sintering of alumina. J Am Ceram Soc 85:1921–1927
23. Lajtai EZ (1971) A theoretical and experimental evaluation of the Griffith theory of brittle fracture. Tectonophysics 11:129–156

24. Misyura SY (2018) Evaporation and heat transfer of aqueous salt solutions during crystallization. Appl Therm Eng 139:203–212

# Figures

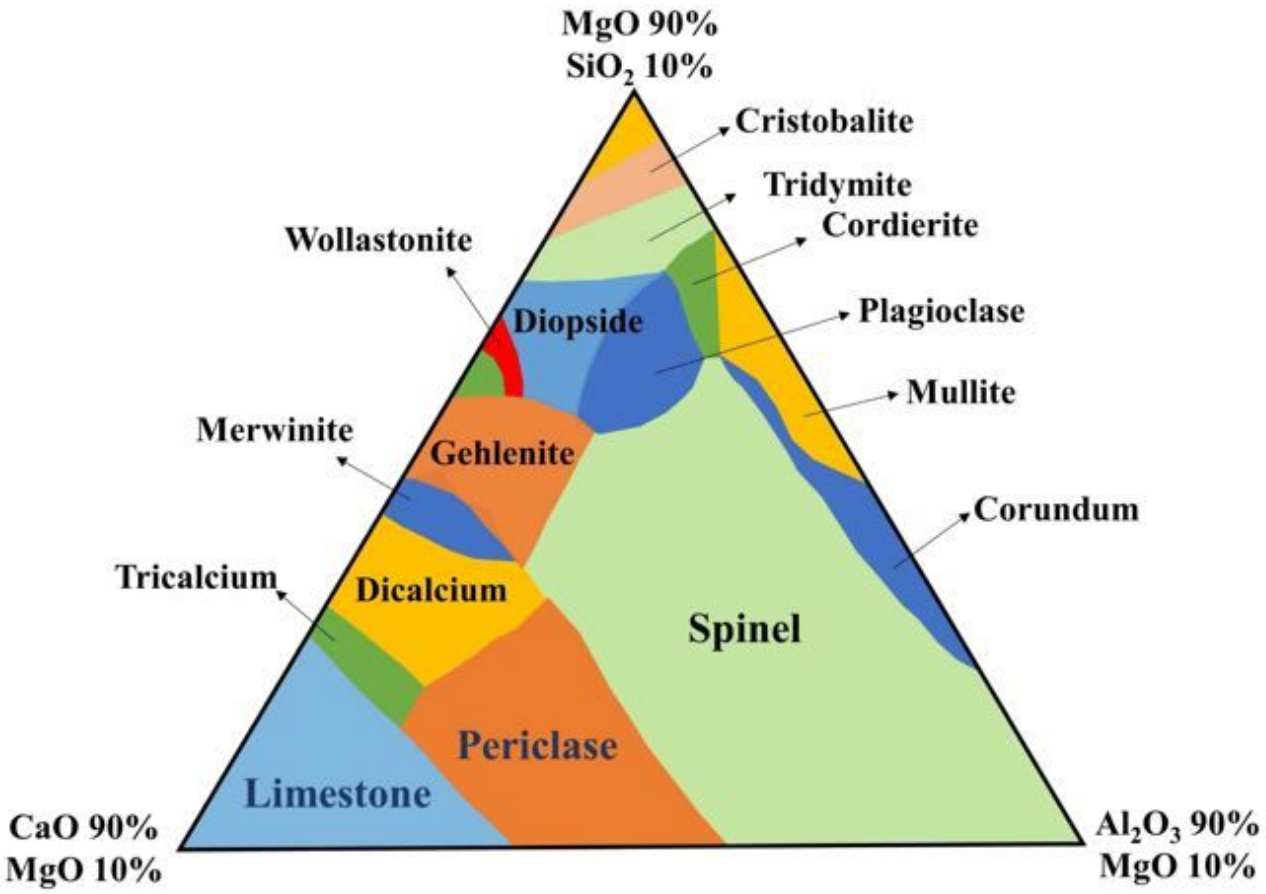


**Figure 1**

The phase diagram of the CaO-Al2O3-SiO2 ternary system containing MgO of 10 wt.%.

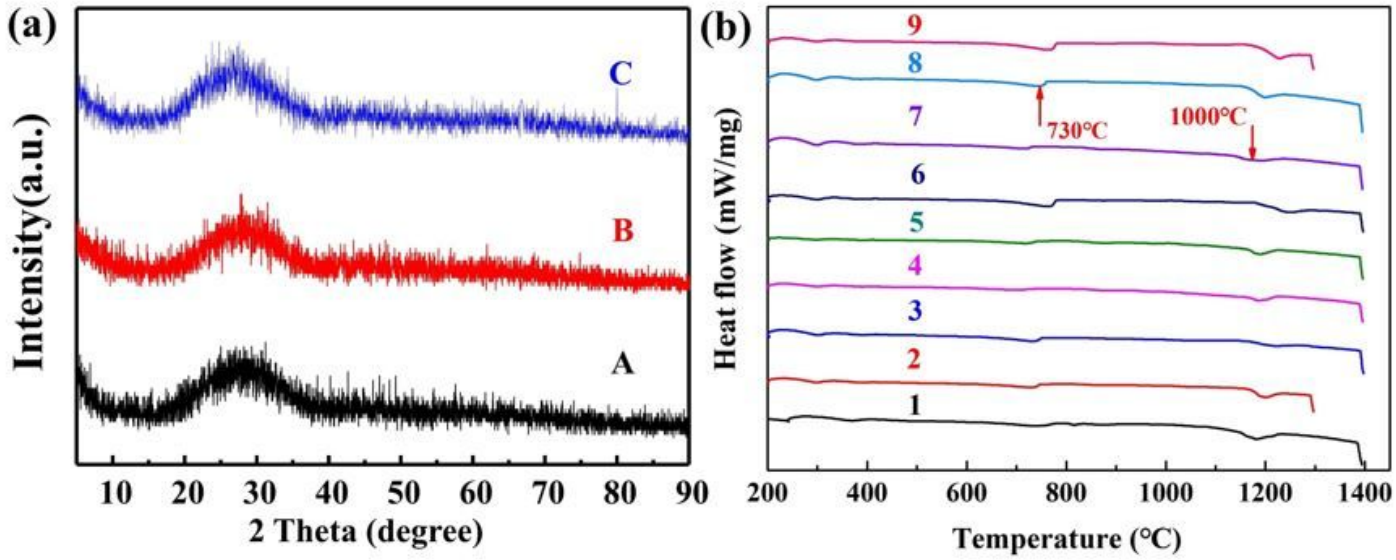


## Figure 2

(a) The XRD pattern of base glass; (b) The DTA curve of based powder

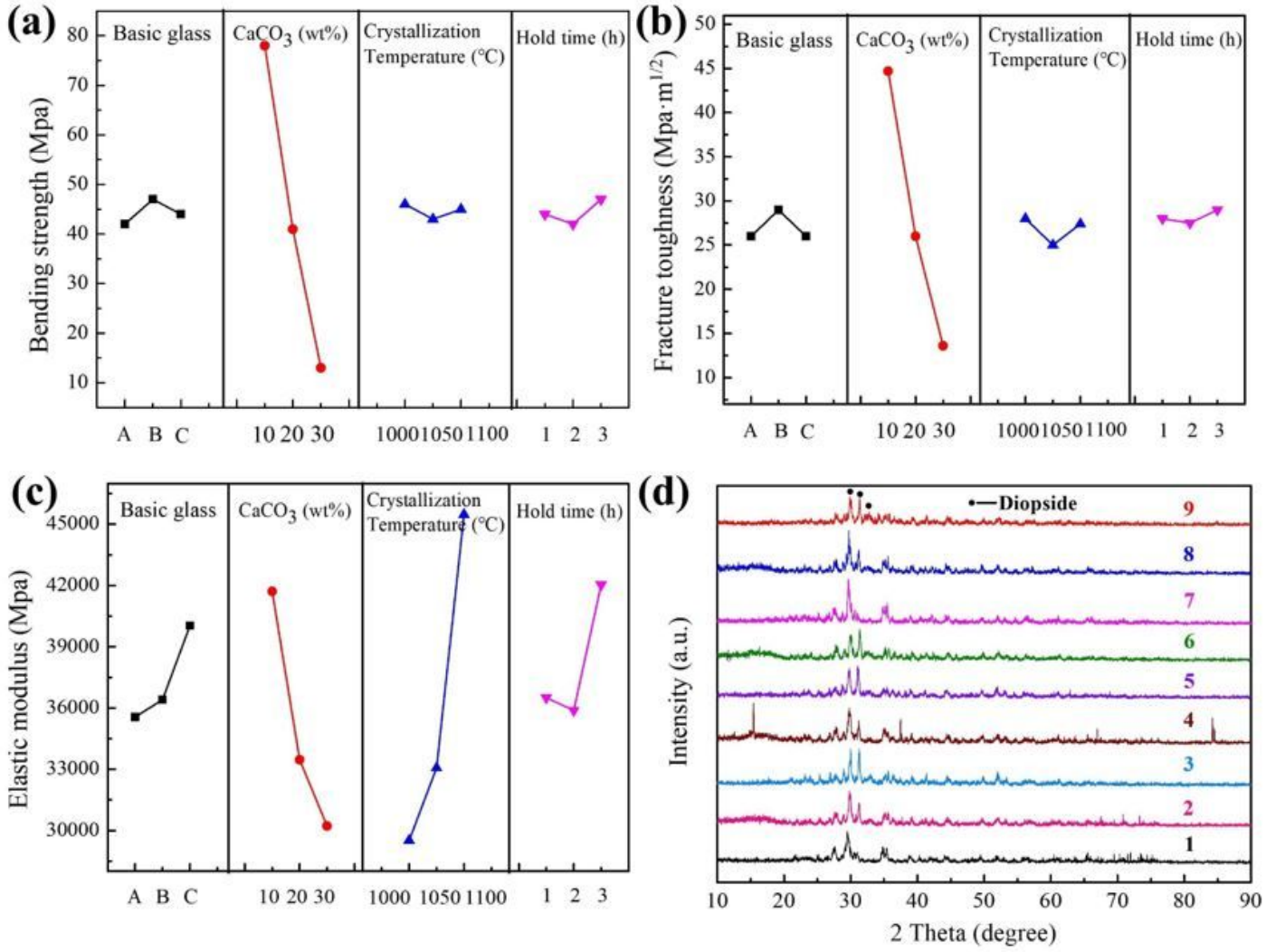

## Figure 3

(a-c) The influence of various factors on the mechanical properties of orthogonal samples; (d) XRD diffraction patterns of orthogonal samples.

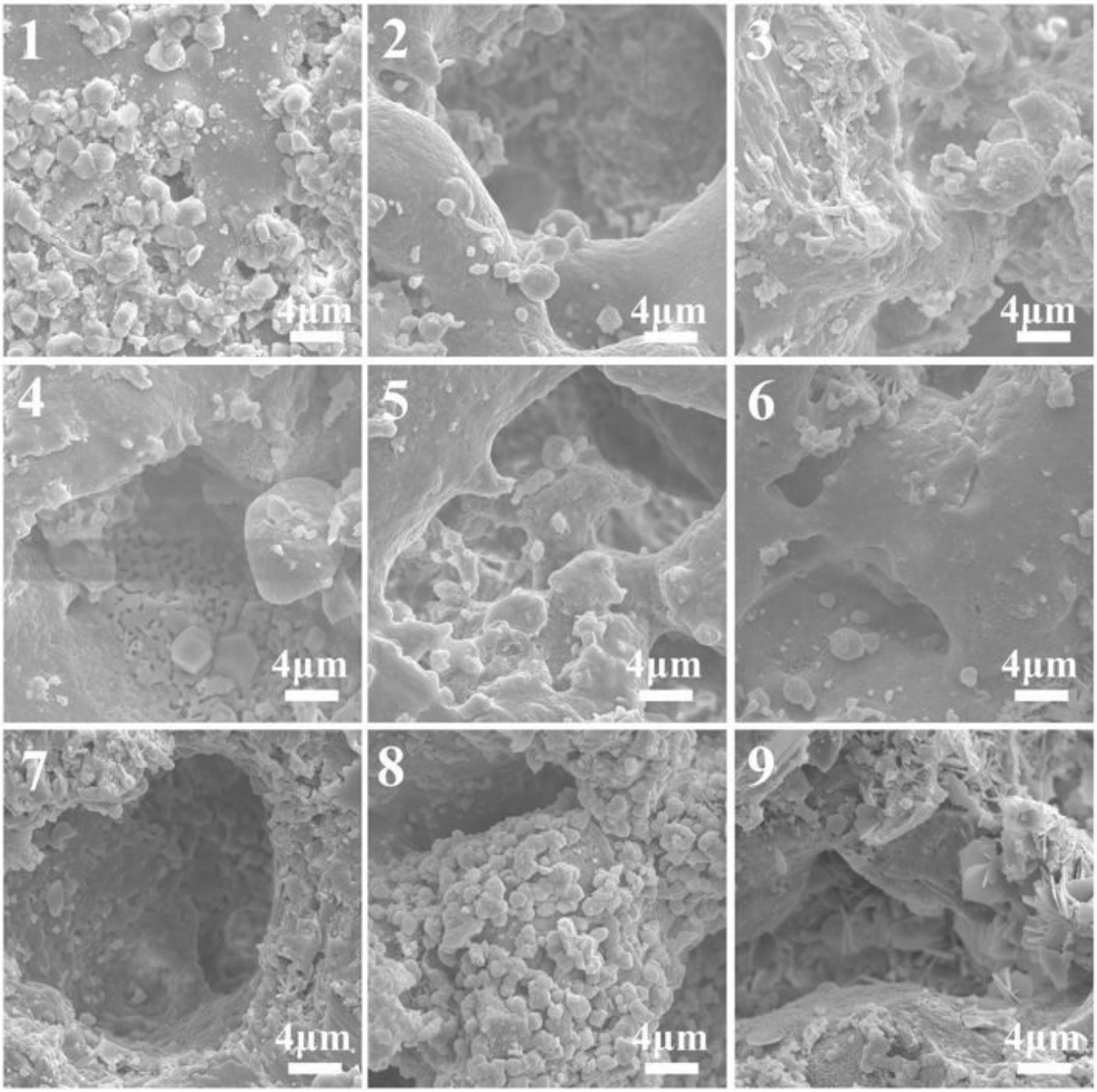


## Figure 4

The XRD diffraction pattern of orthogonal samples (The number represents the corresponding orthogonal experimental sample).

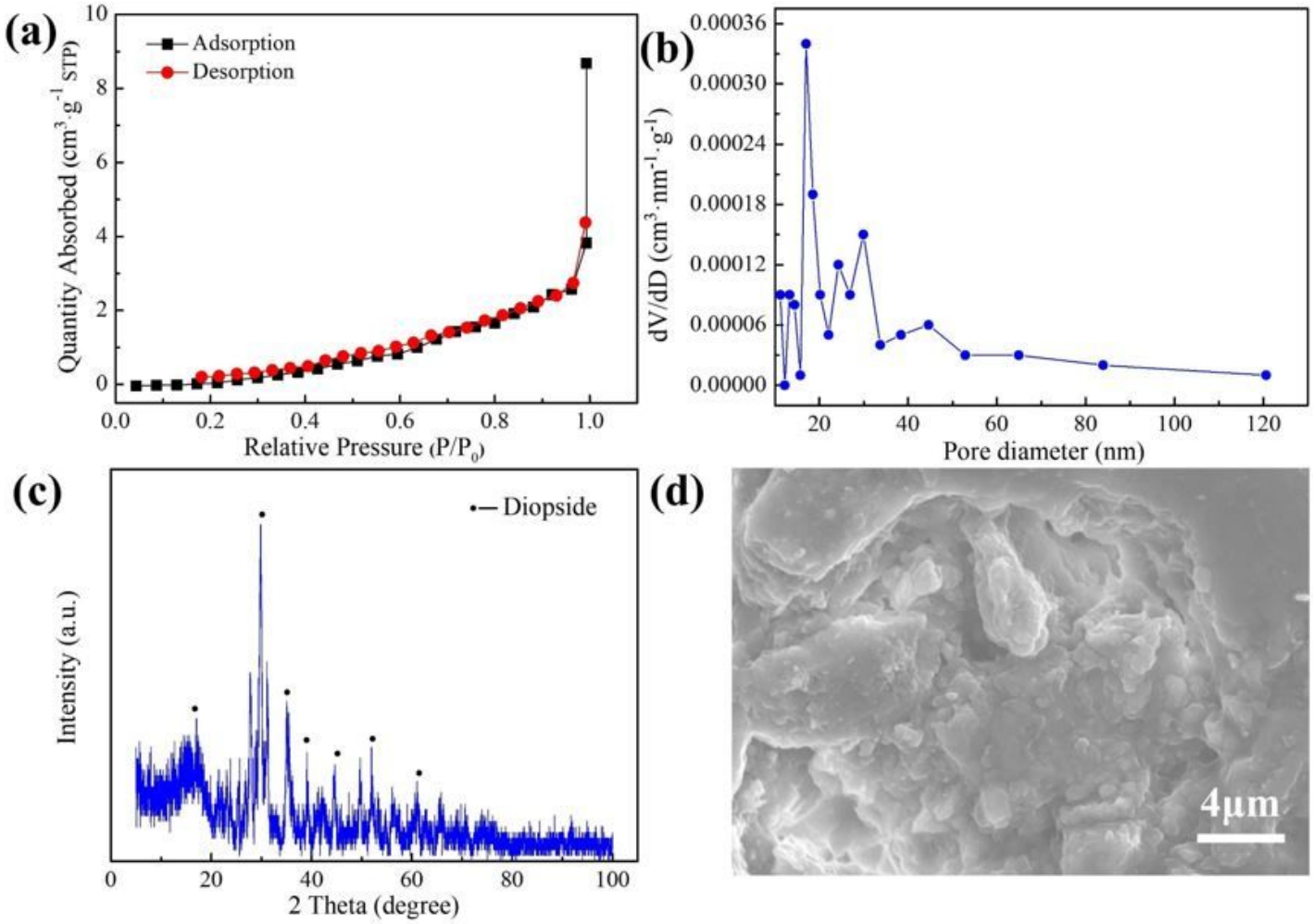


## Figure 5

(a) The adsorption-desorption isotherm curve, (b) the BJH desorption pore size distribution diagram, (c) the XRD pattern, and (d) the SEM image of the sample of the optimized scheme.